Case study

Singularity analysis based on wavelet transform of fractal measures for identifying geochemical anomaly in mineral exploration

Guoxiong Chen [a,b,c], Qiuming Cheng [a,c,*]

[a] State Key Laboratory of Geological Processes and Mineral Resources, China University of Geosciences, Wuhan 430074, China
[b] Faculty of Earth Resources, China University of Geosciences, Wuhan 430074, China
[c] Department of Earth and Space Science and Engineering, York University, Toronto, Canada M3J 1P3

ARTICLE INFO

ABSTRACT

Multi-resolution and scale-invariance have been increasingly recognized as two closely related intrinsic properties endowed in geofields such as geochemical and geophysical anomalies, and they are commonly investigated by using multiscale- and scaling-analysis methods. In this paper, the wavelet-based multiscale decomposition (WMD) method was proposed to investigate the multiscale natures of geochemical pattern from large scale to small scale. In the light of the wavelet transformation of fractal measures, we demonstrated that the wavelet approximation operator provides a generalization of box-counting method for scaling analysis of geochemical patterns. Specifically, the approximation coefficient acts as the generalized density-value in density–area fractal modeling of singular geochemical distributions. Accordingly, we presented a novel local singularity analysis (LSA) using the WMD algorithm which extends the conventional moving averaging to a kernel-based operator for implementing LSA. Finally, the novel LSA was validated using a case study dealing with geochemical data (Fe_2O_3) in stream sediments for mineral exploration in Inner Mongolia, China. In comparison with the LSA implemented using the moving averaging method the novel LSA using WMD identified improved weak geochemical anomalies associated with mineralization in covered area.

© 2015 Elsevier Ltd. All rights reserved.

1. Introduction

The occurrence of ore deposit is often accompanied with various types of geoanomalies, such as geophysical and geochemical anomalies. Delineating geochemical anomalies has become a common practice in geochemical exploration for prospecting mineral deposits (Cheng et al., 1994; Carranza, 2008; Cheng, 2008, 2012a). Recently, the concealed ore deposits in the covered areas (e.g., desert, regolith and vegetation) have drawn increasing attentions of economical geologists, but prospecting this type of ore deposits also brings challenges when using geochemical exploration methods (Cheng, 2012b). Specifically, the elements concentrations caused by underlying mineralization in deeply weathered and transported surface media, especially in those consisting of relatively young sediments, can be so low due to the decay of concentration through such covers that it cannot be easily detected by ordinary sampling and analytical techniques (Cheng, 2012b, 2014). Hence, identification of weak and complicated

geochemical anomalies in covered area brings the crucial challenges to geochemical exploration in support of the mineral resource prediction. Several recently published literatures have reviewed geochemical exploration methods in the past decades (e.g., Singer and Kouda, 2001; Carranza, 2008; Garrett et al., 2008; Cohen et al., 2010; Coker, 2010; Grunsky, 2010; Anand and Robertson, 2012; Cheng 2012b), and much emphasis has been placed on new models for geochemical dispersion from deeply buried mineralization, new sampling and analytical techniques to enhance anomalies, and new mathematical models and geoinformatics techniques for processing and interpreting geochemical anomalies. Among them Cheng (2012b) pointed out that the conventional approaches to identify geochemical anomalies only considering their magnitudes may have some limitations when applied in covered areas mainly due to the complicated signatures of such anomaly patterns.

With the enlightenment of nonlinear science and complexity theories in past decades, numerous articles (e.g., Cheng et al., 1994; Cheng, 2012b; Agterberg, 2014) argued that more complicated properties such as geometry, scaling, singularity, anisotropy and self-similarity should be considered to extract and delineate the geochemical anomalies. Fractal/multifractal concepts,

* Corresponding author at: State Key Laboratory of Geological Processes and Mineral Resources, China University of Geosciences, Wuhan 430074, China.
E-mail addresses: chengxhg@163.com (G. Chen), qiuming@yorku.ca (Q. Cheng).

developed and popularized by Mandelbrot (1967, 1989), provide a powerful tool for modeling and analyzing these complicated nonlinear properties endowed in nature. Recent studies have demonstrated that not only the mineral deposits are scaling distributed (e.g., Mandelbrot, 1989; Bölviken et al., 1992; Agterberg, 1995; Cheng, 1995; Turcotte, 2002), but also the resulting geochemical distributions manifest fractal/multifractal natures (e.g., Cheng et al., 1994; Agterberg and Cheng, 1999; Cheng, 2008; Afzal et al., 2010; Agterberg, 2012; Afzal et al., 2013b). Many fractal models have been proposed and significantly facilitated the pattern recognition and spatial information extraction of complex geochemical landscapes, such as number–size (N–S) model (Mandelbrot, 1983), concentration–area (C–A) model (Cheng et al., 1994), spectrum–area (S–A) model (Cheng et al., 2000), concentration–distance (C–D) model (Li et al., 2003), and concentration–volume (C–V) model (Afzal et al., 2011; Afzal et al., 2013a). Particularly, local singularity analysis (LSA) based on density–area fractal model (Cheng, 1999, 2007, 2012b) has developed as one of the most sophisticated methods to extract weak geochemical anomalies for characterizing singular mineralization and predicting locations of ore deposits (see e.g., Gonçalves, 2001; Cheng and Agterberg, 2009; Arias et al., 2012; Agterberg, 2014).

Almost rising in the same period in 1980s with fractal/multifractal concepts, wavelet transformation (WT) has significantly fascinated the scientific research and engineering application due to its capability for multiscale analyzing objects and localizing signals in both space and frequency domain (Morlet et al., 1982; Daubechies, 1992; Kumar and Foufoula, 1997; Mallat, 1999), so called "numerical microscope" in signal and image processing field. The WT uses a nonlinear approximation scheme with adaptive geometry in contrast with Fourier transformation using linear scheme, so it has a better performance on modeling and analyzing nonstationary or irregular signals (Mallat, 1999). Moreover, an essence of WT is "to see the wood and the trees", i.e., to obtain multiscale natures of the signal through the wavelet-based multiscale decomposition (WMD) algorithm, which provides a promising approach for multiscale decomposing fractal measures to depict the scale-invariance or self-similarity across scales. The WT has been suggested as a natural tool for investigating the interscale relationship of fractal measures because of the inherent scaling property of the wavelet basis (e.g., Arneodo et al., 1988; Muzy et al., 1994; Arneodo et al., 1995; Chamoli et al., 2007; Wendt et al., 2009). There exist an increasing number of research literatures applying WT together with fractal concept for singularity detection (Mallat and Hwang, 1992), stochastic process modeling (Basseville et al., 1992) and image compression (Davis, 1998), to name but a few examples.

The WT has not yet been specifically employed to analyze the multiscale natures of fractal geochemical patterns especially for the scaling analysis of singular geochemical distribution. In the present paper, we aim to apply the WMD to decompose geochemical anomalies and investigate the multiscale component of geochemical landscapes, and special intention is devoted to explore the scaling properties mirrored by wavelet approximations. We argue that the wavelet approximation operator could be regarded as a generalized density–area fractal model for analyzing the singular geochemical distribution. Accordingly, a novel LSA algorithm using WMD could be constructed, which would address the drawbacks of moving averaging involved in implementation of conventional LSA.

This paper is organized as follows: Section 2 reviews the fractal/multifractal theory for modeling singular geochemical distribution and singularity mapping technique for processing geochemical data. Section 3 simply recalls the methodology of WMD, elaborates on the scaling analysis of fractal measures revisited with wavelets and outlines a novel LSA algorithm using WMD.

Section 4 uses a case study dealing with the identification of the weak geochemical anomalies associated with mineralization in Inner Mongolia (China) to validate the proposed LSA. Section 5 draws the conclusions.

2. Singularity theory and method for mapping geochemical anomaly

2.1. Fractal and singularity

In order to understand how the fractal/multifractal theory can be applied to model and analyze the natures of geochemical anomalies, we briefly recall herein the basic concepts of fractals. A key feature of fractal is scale-invariance, which is intimately tied to a power–law type of proportionally relation between a measure $M(\delta)$ and the measure scale δ

$$M(\delta) \propto \delta^{E-D}, \tag{1}$$

where $\propto$ stands for proportionally. E, D and $E-D$ represent topological dimension, fractal dimension and fractal codimension (singularity/scaling index), respectively. One of the purposes of fractal/scaling analysis is to detect such power–laws and quantify their exponents that characterize the properties of irregular such as the roughness and singularity. Multifractal modeling quantifies the multiscaling behaviors and characterizes the spatial distribution of singularities.

Fractal/multifractal, as a nature consequence of self-similarity (Mandelbrot, 1983, 1989; Evertszy and Mandelbrot, 1992), has been widely used to describe, analyze and model various types of singular geo-processes, such as earthquakes, hurricanes, floods, volcanoes, landslides and mineralization (Cheng, 2008, 2012b). Such singular geo-processes often result in anomalous amounts of energy release or mass accumulation confined to narrow intervals in space or time, which is termed as singularity (Cheng, 2007). Singularity is the generic property of fractal/multifractal products generated by nonlinear natural process. Mineralization resulting from the hydrothermal process in the Earth's crust can be considered as a general type of singular geo-process that can result in extreme enrichment of metals in form of ore deposits (Cheng, 2007, 2012b). This singular phenomenon is often observed in the spatial distribution of geochemical concentrations in secondary media (e.g., stream sediments, soil, tills and water) caused by underlying mineralization (Cheng, 2007; Agterberg, 2014; Cheng, 2014).

2.2. Density-area fractal model and singularity analysis

From a generalized fractal point of view, the fractal/singular geochemical distribution can be described as the following power–law relationship between the total amount of element $\mu(\varepsilon)$ and a ε-radius sampling box $B(\varepsilon) \subset \mathbb{Z}^n$

$$\mu(\varepsilon) = \int_{B(\varepsilon)} d\mu \simeq c\varepsilon^{\alpha}, \tag{2}$$

where α is known as the singularity index, and c is a constant called fractal density (Cheng, 2015). Define $\rho(\varepsilon)$ representing the generalized element density-value of $\mu(\varepsilon)$ in box $B(\varepsilon)$ with $\rho(\varepsilon) = \int_{B(\varepsilon)} \chi_{B(\varepsilon)} d\mu$, where $\chi_{B(\varepsilon)}$ is a probability density function within the box. If $\rho(\varepsilon)$ denotes the arithmetic average of $\mu(\varepsilon)$ for 2D geochemical data, then the density–area fractal model proposed by Cheng (1999) can be obtained as

$$\rho(\varepsilon) = \int_{B(\varepsilon)} \varepsilon^{-2} d\mu \simeq c\varepsilon^{\alpha-2}. \tag{3}$$

Above model is often used to map the spatial distribution of singularity index of 2D geochemical pattern. The singularity indices for indicating geochemical anomaly can be divided into three cases: (1) $\alpha < 2$ indicates high concentration or enrichment of elements, showing positive singularity; (2) $\alpha > 2$ indicates low concentration or deficit of elements, showing negative singularity; (3) $\alpha \approx 0$ indicates background field with non-singular. Several recent studies have demonstrated that singularity index acts as a powerful high-pass filter for extracting weak geochemical or geophysical anomalies from complicated background field, and the LSA is particular helpful for discovering concealed ore deposits or other buried geological bodies (e.g., Ali et al., 2007; Zuo et al., 2009; Wang et al., 2011; Chen et al., 2015; Chen et al., 2013).

The LSA or singularity mapping can be implemented by different methods such as regular/irregular windows, contours and geological units defined by integrated layers of geological patterns (Cheng, 2006, 2012b). Among them the simplest form is the square window-based box-counting algorithm (Cheng and Agterberg, 2009). The density-value $\rho(\varepsilon_i)$ are obtained from the average value within a series of window size $\varepsilon_{\min} = \varepsilon_1 < \varepsilon_2 < ... < \varepsilon_i = \varepsilon_{\max}$ for any given sampling point on the map. This process is equivalent to the multiscale moving averaging (MA) which results in a suit of $\rho(\varepsilon_i)$, and these density-values at same point satisfy a power–law scaling whose index quantifies the singularity strength. From the definition of Eq. (3), it would become straightforward to understand that the multiscale density measures are obtained by convolving geochemical data with a suit of box function (viz., the reciprocal of box numbers). However, it is well known that MA algorithm employs a linear averaging scheme for characterizing geochemical variables within the window, and it often ignores the complex features of geochemical patterns. In practice, it would be ill-suited for processing nonstationary anomalies especially for those non-isolated singularities. In the subsequent section, we would like to introduce a generalized box-counting algorithm provided by WMD for analyzing geochemical measures and calculating element density-value.

3. Local singularity analysis revisited with wavelets

3.1. Wavelet transformation and multiscale decomposition

The continuous wavelet transformation (CWT) of a function $f(\mathbf{x}) \in L^2(\mathbb{Z}^n)$ at scale a (related to wavelength) and position $\mathbf{b}$ is computed by correlating $f(\mathbf{x})$ with a wavelet atom (Grossmann and Morlet, 1984) as following

$$\mathbf{W}f_\psi(a, \mathbf{b}) = \frac{1}{a^n} \int_{-\infty}^{+\infty} f(\mathbf{x})\psi\left(\frac{\mathbf{x} - \mathbf{b}}{a}\right)d\mathbf{x}, \quad a > 0, \quad \mathbf{x} \in Z^n,$$
$$\mathbf{b} \in \mathbb{Z}^n, \tag{4}$$

where $\psi_{a,\mathbf{b}}$ defines a family of isotropic wavelet obtained by translation and dilation of the mother wavelet $\psi(\mathbf{x}) \in L^2(\mathbb{Z}^n)$. Note that L^1-norm $(1/a)$ has been used in Eq. (4) for normalization. Eq. (4) can be further considered as a convolution product: $\mathbf{W}f_\psi(a, \mathbf{b}) = f*\psi_a(\mathbf{b})$, thereby decomposing the function $f(\mathbf{x})$ into elementary space-scale contribution by convolving it with a suit of mother wavelets which are well localized in space and frequency. Fig. 1 shows a tiling of space-frequency plane defined by a 1D wavelet basis. The shape of a wavelet resolution adaptively depends on the scale. As the scale decreases, the space support is reduced but the frequency spread increases. It suggests that the resolution of WT can be improved adaptively for analyzing high-frequency signal, while become poor for analyzing low-frequency signal. The zooming capability of the wavelet transformation not only can locate isolated singularity events, but can also
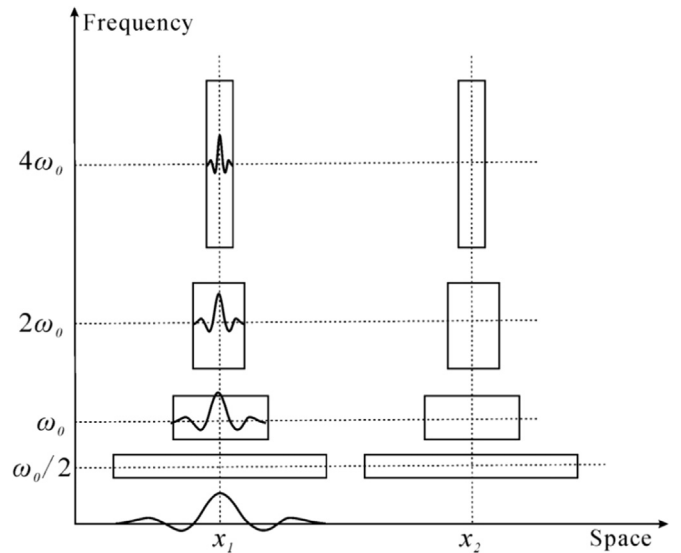

Fig. 1. Multiresolution space-frequency tilling of wavelet analysis. The shape of a wavelet resolution adaptively depends on scale.

characterize more complex multifractal signals possessing non-isolated singularities (Mallat and Hwang, 1992; Mallat, 1999).

The framework of WMD is introduced by Mallat (1989a,b) to project signal $f(\mathbf{x})$ onto a set of basis $\{\varphi_{J,k}(\mathbf{x}), \{\psi_{j,\mathbf{k}}^{(i)}(\mathbf{x})\}_{j \leq J}\}, \quad j \in \mathbb{Z}, \quad \mathbf{k} \in \mathbb{Z}^n, \quad i = 1, 2, ...2^n - 1$, where

$$\psi_{j,\mathbf{k}}^{(i)}(\mathbf{x}) = 2^{-jn}\psi^{(i)}(2^{-j}\mathbf{x} - \mathbf{k}), \tag{5}$$

and $\varphi_{j,\mathbf{k}}(\mathbf{x}) = 2^{-jn}\varphi(2^{-j}\mathbf{x} - \mathbf{k}),$ (6)

are obtained by dilating and translating the mother wavelet $\psi(\mathbf{x})$ and father wavelet (scaling function) $\varphi(\mathbf{x})$, respectively, with the special choice $a = 2^j$ and $\mathbf{b} = 2^j\mathbf{k}$ for discretization. The WMD is realized using a simple scheme, the so-called pyramid algorithm (Fig. 2). More details about the WMD algorithm can be found in Mallat (1989a,b). Hence, the signal $f(\mathbf{x})$ can be represented as

$$f(\mathbf{x}) = \sum_{\mathbf{k} \in \mathbb{Z}^n} A_{\mathbf{k}}\varphi_{j,\mathbf{k}}(\mathbf{x}) + \sum_{j=1}^{J} \sum_{\mathbf{k} \in \mathbb{Z}^n} \sum_i d_{j,\mathbf{k}}^{(i)}\psi_{j,\mathbf{k}}^{(i)}(\mathbf{x}) \tag{7}$$

with $A_{\mathbf{k}}^j = \int f(\mathbf{x})\varphi_{j,\mathbf{k}}(\mathbf{x})d\mathbf{x}$ and $d_{j,\mathbf{k}}^{(i)} = \int f(\mathbf{x})\psi_{j,\mathbf{k}}^{(i)}(\mathbf{x})d\mathbf{x}$ are termed as
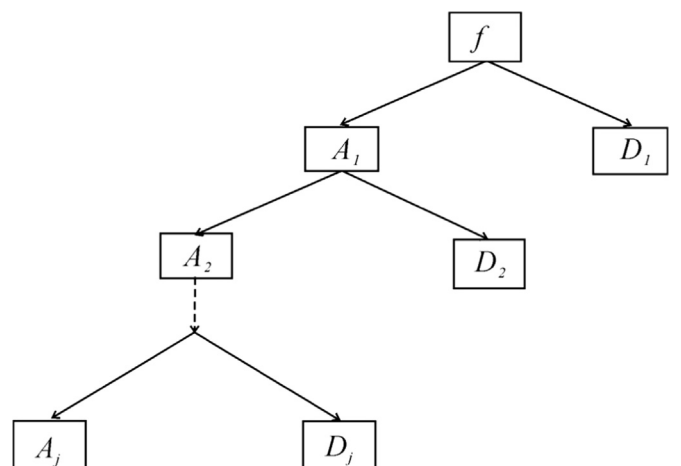

Fig. 2. Pyramid architecture of the multiresolution analysis. Details and approximations are progressively built in pyramid from up to scale j.

approximation coefficient and detail/wavelet coefficient, respectively. For instance, the multiscale representation of 2D signal $f(\mathbf{x})$ up to scale J consists of a low-resolution approximation $A_{\mathbf{x}}^{J}$ and three high-frequency details $D_{j,\mathbf{k}}^{(i)}$, $i = 1, 2, 3$ in horizontal-, vertical- and diagonal-direction.

3.2. Scaling analysis of fractal measures with wavelets

For a fractal measure defined in Eq. (2), it has following scaling property at the vicinity of a singular point $\mathbf{x}_0 \in \mathbb{Z}^n$

$$\mu_{\mathbf{x}_0}(\lambda\varepsilon) \sim \lambda^{\alpha(\mathbf{x_0})}\mu_{\mathbf{x}_0}(\varepsilon), \tag{8}$$

where λ is a scalar number. In order to multiscale analyze fractal measures, the wavelet transform can be used to decompose $\mu(\mathbf{x})$ as

$$\mathbf{W}f_{\psi}(a, \mathbf{b}) = \frac{1}{a^n} \int \psi\left(\frac{\mathbf{x} - \mathbf{b}}{a}\right) d\mu(\mathbf{x}), \quad \mathbf{b} \in \mathbb{Z}^n. \tag{9}$$

It has been shown that by using mother wavelet $\psi(\mathbf{x})$ the scaling behavior $c|\mathbf{x} - \mathbf{x_0}|^{\alpha(\mathbf{x_0})}$ of singular function $f(\mathbf{x})$ can be mirrored by detail/wavelet coefficients (Arneodo et al., 1988; Muzy et al., 1994; Wendt et al., 2009). However, for scaling analysis of fractal/singular measures $\mu(\mathbf{x})$ defined in Eq. (2), it is more suitable by using father wavelet $\varphi(\mathbf{x})$ since it satisfies the general condition: $\int_{-\infty}^{\infty} \varphi(\mathbf{x}) d\mathbf{x} = 1$, which is equivalent to a box function (i.e., a characteristic function of box). Therefore, the Eq. (9) using father wavelet (scaling function) computes the value of approximation coefficient $A_{\mathbf{x}}^{j}$.

According to the way that proved the scaling properties of wavelet coefficient in Arneodo et al. (1988), it can be readily deduced that the scaling behavior of fractal measure $\mu(\mathbf{x})$ in Eq. (8) can be mirrored by approximation coefficient as

$$\mathbf{W}f_{\varphi}(\lambda a, \mathbf{x_0}) \sim \lambda^{\alpha-n}\mathbf{W}f_{\varphi}(a, \mathbf{x_0}), \quad \mathbf{x_0} \in \mathbb{Z}^n. \tag{10}$$

Here, we just give a succinct proof using the dyadic WT of fractal measures as following:

$$\begin{aligned}A_{\mathbf{k}}^{j} &= 2^{-jn} \int \varphi_{j,\mathbf{k}}(2^{-j}\mathbf{x} - \mathbf{k}) d\mu(\mathbf{x}), \quad \text{with} \quad \mathbf{x}' = 2\mathbf{x} \\ &= 2^{-\alpha} \int 2^{-jn}\varphi_{j,\mathbf{k}}(2^{-(j+1)}\mathbf{x}' - \mathbf{k}) d\mu(\mathbf{x}') \\ &= 2^{n-\alpha} \int 2^{-(j+1)n}\varphi_{j,\mathbf{k}}(2^{-(j+1)}\mathbf{x}' - \mathbf{k}) d\mu(\mathbf{x}') \\ &= 2^{n-\alpha}A_{\mathbf{k}}^{j+1}. \end{aligned} \tag{11}$$

For 2D measure $\mu(\mathbf{x})$, in considering $n = 2$ the approximation coefficients $A_{\mathbf{x}}^{j}$ at singular point $\mathbf{x_0}$ scale like

$$A_{\mathbf{x}_0}^{j+1} = 2^{\alpha(\mathbf{x}_0)-2}A_{\mathbf{x}_0}^{j}, \, \mathbf{x}_0 \in \mathbb{Z}^2. \tag{12}$$

Thus, the local singularity strength $\alpha(\mathbf{x_0})$ can be estimated as

$$\alpha(\mathbf{x_0}) = \log_2(A_{\mathbf{x}_0}^{j+1}/A_{\mathbf{x}_0}^{j}) + 2. \tag{13}$$

The father wavelet plays a role of generalized box, so the resulting wavelet approximation coefficients $A_{\mathbf{x}}^{j}$ of signal $f(\mathbf{x})$ provide a natural generalization of the classical box-counting method for multiscale analyzing the fractal measures. Furthermore, the $A_{\mathbf{x}}^{j}$ can be regarded as a convolution product $f * \varphi_j(\mathbf{k})$, namely the realization of weighted moving averaging in which the weighted function is derived from orthonormal basis $\varphi_{j,\mathbf{k}}$. Therefore, the approximation coefficient $A_{\mathbf{x}}^{j}$ obtained from WMD may equivalently quantify the generalized areal density-value $\rho(\varepsilon)$ defined in model (3), since it depends on the weighted average value of $f(\mathbf{x})$ within a 2^j-radius square box. Consequently, the approximation coefficients can be employed to rewrite the density–area fractal model in Eq. (3) as

$$A_{\mathbf{x}}^{j} \simeq c(2^{j})^{\alpha(\mathbf{x})-2}. \tag{14}$$

Above model shows homologous scaling properties with Eq. (13) and could provide a generalized power–law relation for modeling the singular geochemical distributions.

3.3. Singularity mapping algorithm using wavelet transformation

With the local singularity analysis, the spatial distribution of singularities plays an important role in investigating the local structure of geochemical pattern and finding potential locations of ore deposits. Here, we proposed a novel local singularity analysis (singularity mapping) algorithm using WMD for processing 2D geochemical pattern in supporting mineral exploration, as follows.

(i) First compute the multiscale approximation coefficients $A_{\mathbf{x}}^{j}$ ($j = 1, 2, 3, …, J$) by using the undecimated wavelet transform (i.e., stationary wavelet transform, SWT) of 2D geochemical data. The code for 2D SWT used for obtaining pointwise $A_{\mathbf{x}}^{j}$ in this manuscript is modified from wavelet toolbox in MATLAB to avoid coordinate shifting. There exist a certain number of families of father wavelets, and it should be noted that the novel LSA algorithm using Haar wavelet can be regarded as the realization of conventional LSA.

(ii) Estimating the local singularity index according to the logarithmic transformation of Eq. (14) yielding: $\log_2(A_{\mathbf{x}}^{j}) \simeq \log_2 c + (\alpha(\mathbf{x}) - 2)j$. For a location on the map, the slope estimated from the linear relationship between $A_{\mathbf{x}}^{j}$ and j on log–log paper by using linear regression analysis can be considered as the estimate of $(\alpha - 2)$. Then the 2D distribution of singularity strength can be mapped straightforward. The uncertainty related to the estimation of singularity index also can be recorded and mapped to evaluate the reliability of singularity mapping result.

Several benefits can be achieved from using the proposed LSA based on WMD for mapping geochemical anomalies. First it provides a generalization of box-counting method for scaling analysis of fractal/singular geochemical measure, and the choice of the box function derived from orthonormal basis becomes flexible. Second it provides a nonlinear (weighted averaging) scheme instead of linear (averaging) scheme for calculating the element density-value in density–area fractal modeling, thereby getting rid of the possible smooth behaviors that may mask singularities. Third the novel LSA using a fast multiscale decomposition algorithm would spend less numerical computation in comparison with the time-consuming algorithm of the conventional LSA using MA, especially for processing a large dataset.

4. Case study and results

4.1. Geological setting

The Shamai-Chaobuleng mineral district is situated in Inner Mongolia province of the northern China (Fig. 3). This region is composed of 40.2% Quaternary sediments (Q), 33.4% Tertiary sediments (T), 17.0% granites and 9.4% other Formations (Fig. 3). More than 70% of the area is covered by Quaternary and Tertiary sediments. The drilling data revealed that the thickness of Quaternary and Tertiary sediments in this region ranges from 0.5 to 3.0 m and from 42.0 to 77.0 m, respectively (Cheng, 2012b, a; Zuo et al., 2013; Cheng, 2014). The Chaobuleng skarn-type Fe polymetallic deposit is located in the NE which is one of the famous mineral deposits in this region and it is controlled by regional-scale NE trending faults. The mineral assemblages associated with the Fe polymetallic mineralization often have high concentrations
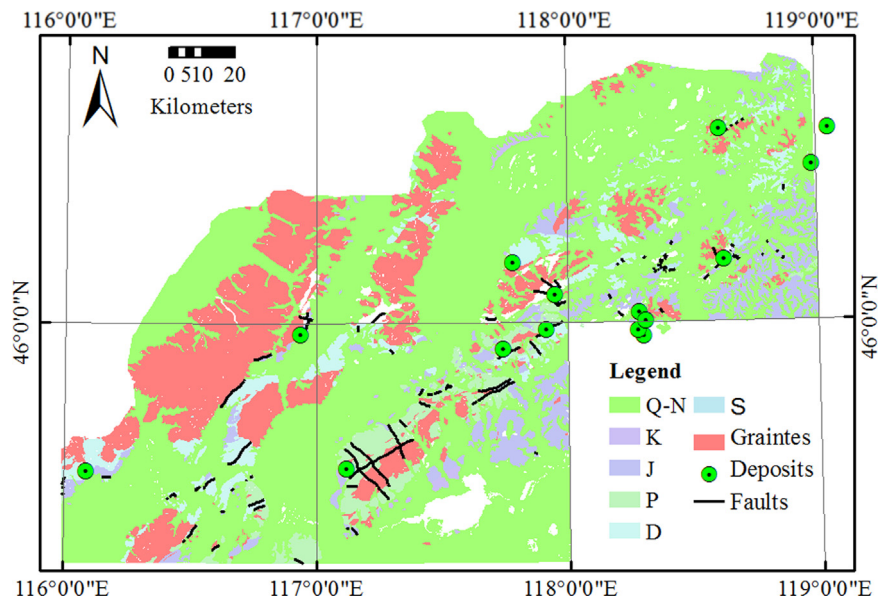
Fig. 3. Simplified geological map of Chabuleng-Shamai, Inner Mongolia of north China (after Zuo, 2013).
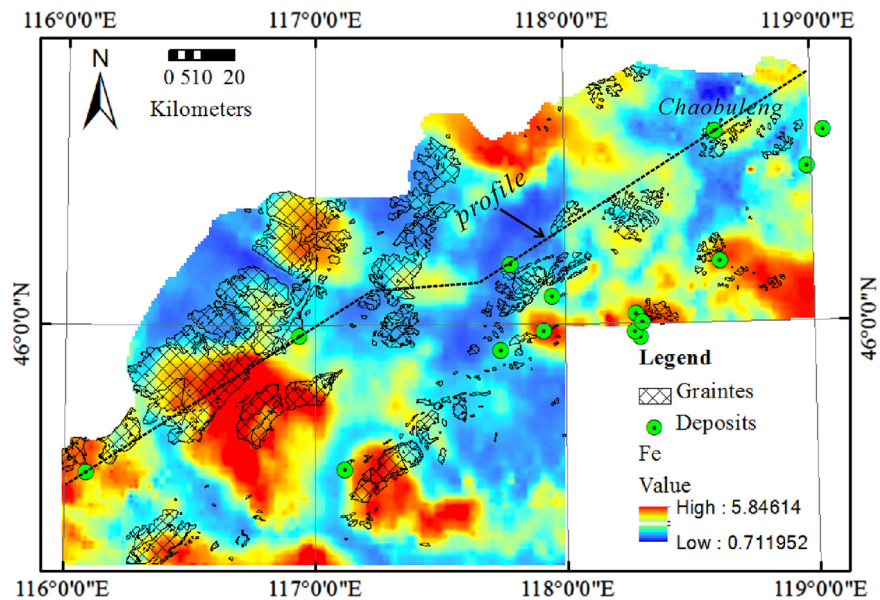

Fig. 4. Spatial distribution patterns of Fe_2O_3 (%)in stream sediments. (For interpretation of the references to color in this figure, the reader is referred to the web version of this article.)

of Fe, Cu, Mo, Ag, As, Pb, Zn, Bi and Ti.

The stream sedimentary geochemical data used in this study were collected and analyzed during the Chinese National Geochemical Mapping (CNGM) project as part of the "Regional Geochemistry National Reconnaissance (RGNR) Project". In this research, one of the main ore-forming compounds, Fe_2O_3, was studied together with LSA to address the identification of weak anomalies caused by buried Fe polymetallic deposit. Fig. 4 shows the raster patterns of Fe_2O_3 (%) with resolution of 1×1 km^2 generated by using the inverse distance weighted (IDW) interpolation. The concentrations of Fe_2O_3 were determined by using X-ray fluorescence and the detection limit for Fe_2O_3 was 0.05%. Logarithmic differences and standard deviations between the analytical values and the recommended values of the standard reference samples are lower than 0.07%.

4.2. Multiscale decomposition of geochemical patterns

Wavelet-based multiscale decomposition is undertaken to decompose 2D geochemical pattern (Fe_2O_3) into multiscale components including approximations and details. There exist a variety of wavelet families in WMD algorithm (e.g., *Haar*, *Daubechies* (*db*), *symlets* (*sym*), and *Biorthogomal*, etc.), and a proper wavelet should be determined for processing geochemical data. Three criteria may influence the choice of wavelet including number of vanishing moments, support size and regularity (Mallat, 1999, p599). The wavelet regularity is crucial for increasing the fidelity of separated components, and higher vanishing moment is better to analyze the singular signals. Considering the fact that the practical geochemical pattern usually presents fractal natures, the regular orthonormal wavelets with higher compact support such as *db* 4–10 and *sym* 4–8, may be better choices for obtaining reasonable decompositions. Consequently, after a test of using
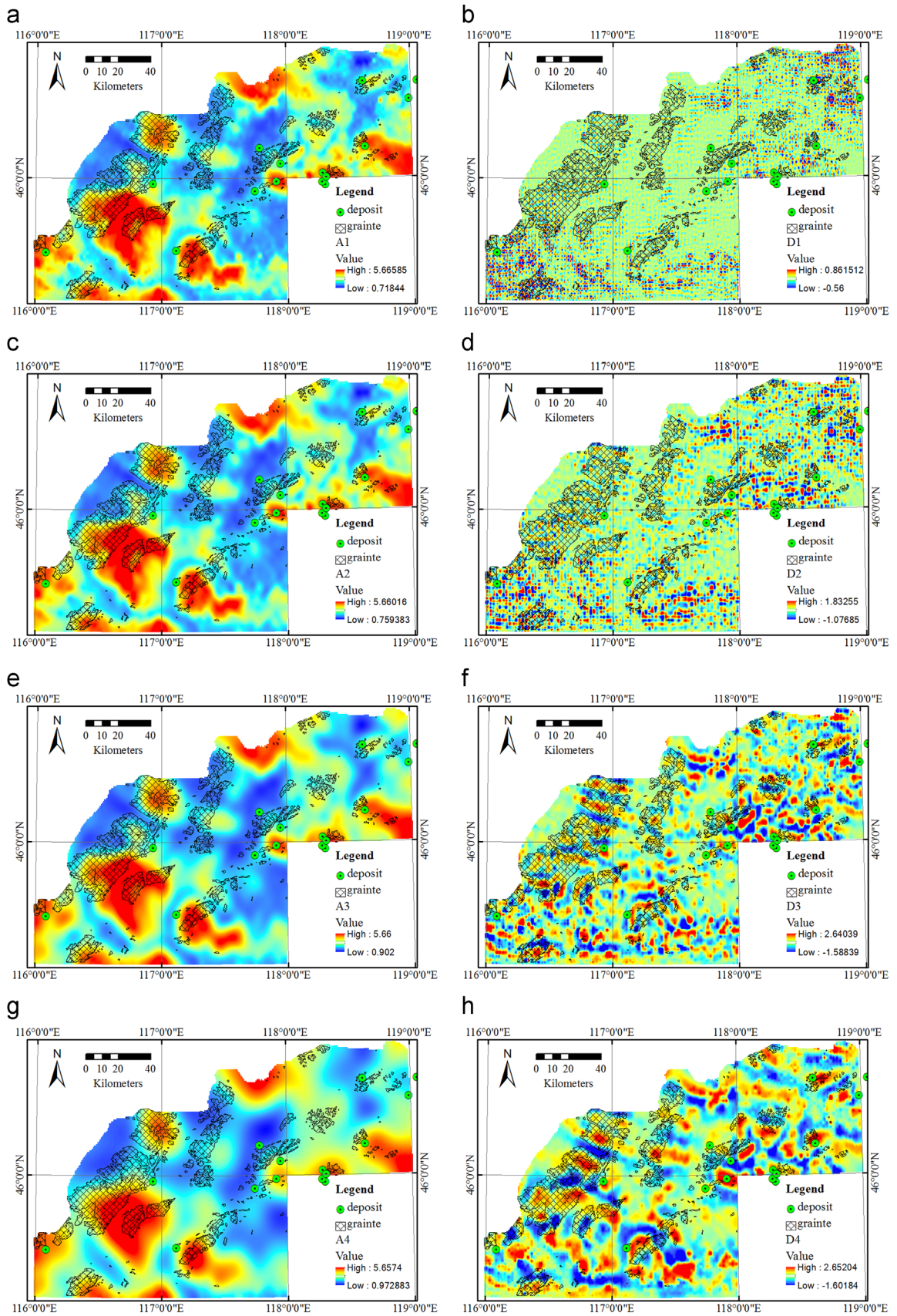
Fig. 5. Multiscale decomposition of geochemical patterns (Fe$_2$O$_3$) using wavelet transformation. (a), (c), (e) and (g) represent the multiscale approximations at scale $j=1$, 2, 3 and 4. (b), (d), (f) and (h) represent the multiscale details at scale $j=1$, 2, 3 and 4.
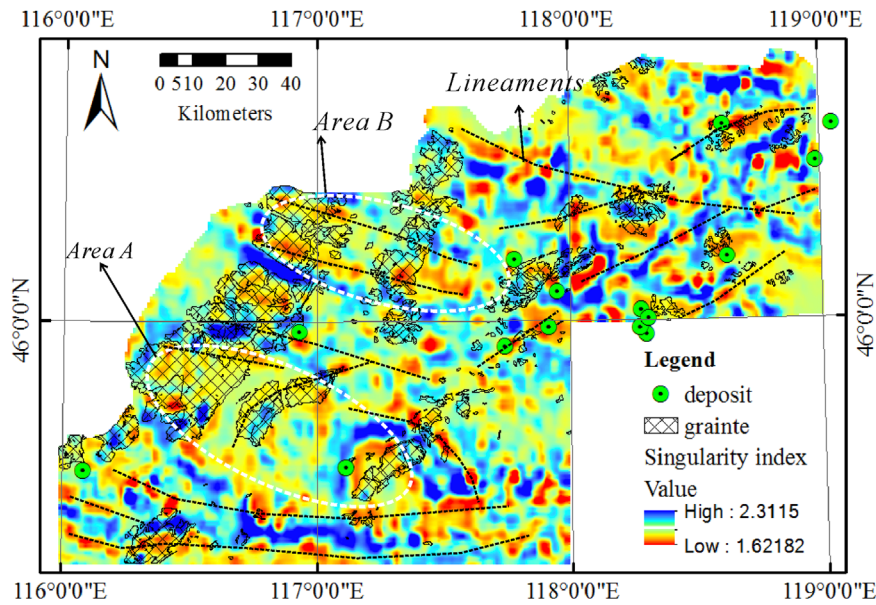
Fig. 6. Map showing the singularity distributions of Fe_2O_3 obtained from the conventional LSA algorithm.
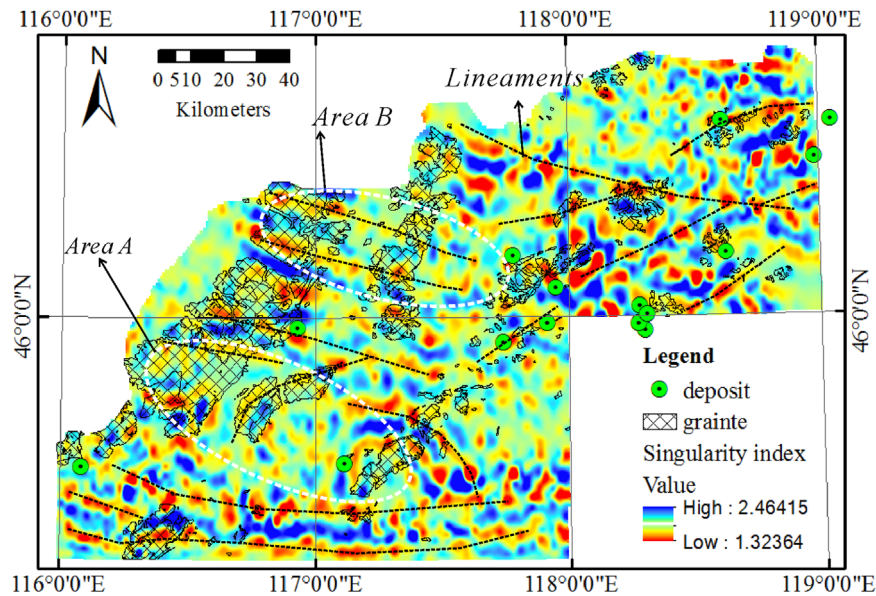

Fig. 7. Map showing the singularity index distribution of Fe_2O_3 obtained from the novel LSA algorithm using WMD.

various wavelet functions, we choose $db8$ wavelet function in WMD for decomposing the geochemical pattern in this study.

Here, the WMD of geochemical pattern (Fig. 4) stops at the 4th decomposition level since the resulting components of further levels do not contain the anomaly details of interests related to local mineralization. Fig. 5a, c, e and g show multiscale approximations of geochemical pattern at scale $j=1$, 2, 3 and 4, respectively, consisting of low-frequency components. These wavelet approximation maps could be regarded as smoothing (averaging) results of original geochemical pattern because of the low-pass filtering of the father wavelet in WMD. Moreover, they show similar geometric patterns with scale increasing essentially due to the power–law dependence of approximation values on the scales. In addition, Fig. 5b, d, f and h show multiscale details of geochemical pattern at scale $j=1$, 2, 3, and 4, respectively. Each detail is the superposition of three high-frequency components in horizontal-, vertical- and diagonal-direction. Notably, more details or

anomalies patterns appear on Fig. 5b, d, f and h compared with original geochemical map (Fig. 4), which is attributed to the high-pass filtering of the mother wavelet in WMD.

It is known that the WMD algorithm could be a powerful tool for decomposing geochemical pattern into multiscale components of different frequency bands from fine scale to coarse scale, then some questions can be raised for geochemical data processing and interpretation in mineral explorations. For instance, Can these multiscale anomalies imply any statistical properties of complex geo-processes? what are the specific geological or geochemical implications of different scale anomalies? Can we use these multiscale natures of geochemical pattern for fractal/scaling analysis? In the subsequent session, we would like to elaborate upon the idea that these multiscale geochemical components possess statistical self-similarity in which the scaling property can help detect the spatial distribution of singularities, and the proposed LSA based on the generalized density–area fractal model in Eq. (14) is
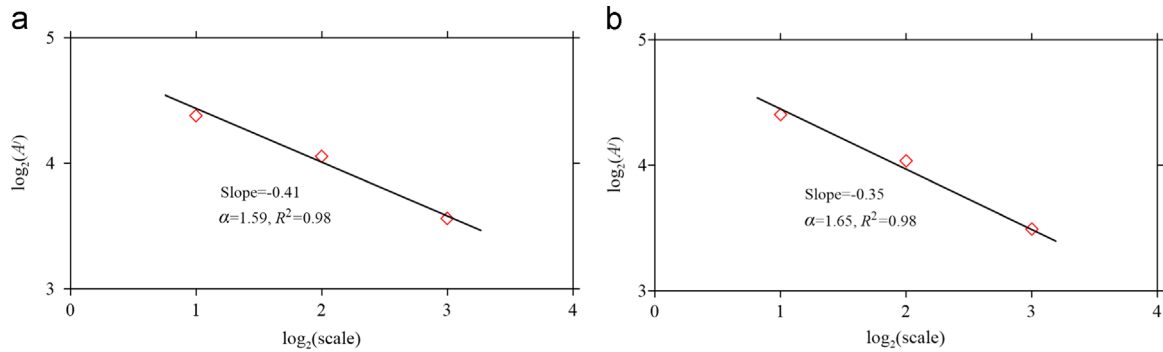
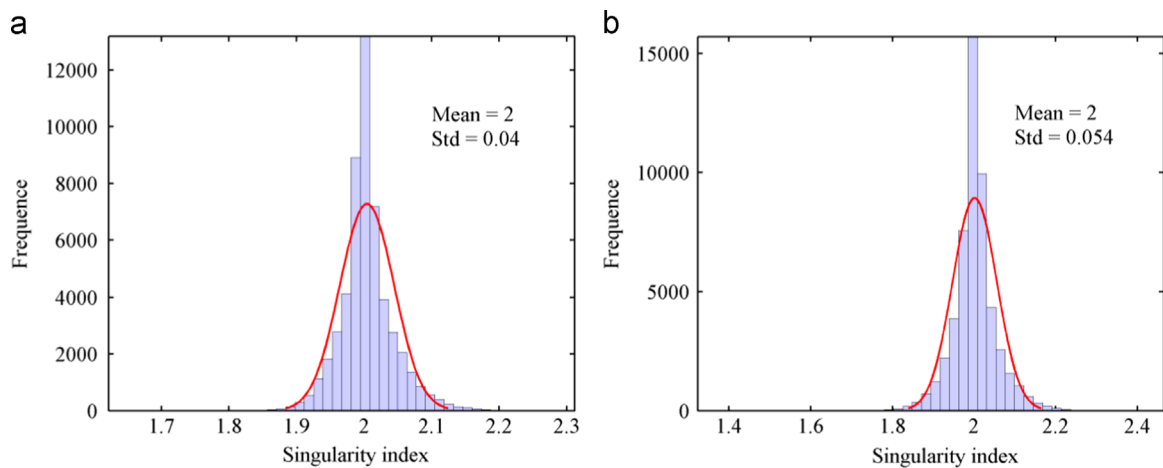**Fig. 8.** Log–log plots of approximation coefficients versus scale (logs based on 2).

Fig. 9. Histogram of singularity indices estimated by (a) the conventional LSA and (b) the novel LSA.

used to quantify the interscale relationship of these multiscale approximations.

4.3. Singularity mapping for identifying weak geochemical anomalies

Since the study area is covered by large-area grasslands, geochemical information are often mashed or weakened by deeply weathered and transported covers. From the spatial distribution of Fe_2O_3 in Fig. 4, it can be observed that the overburden covered areas (green) consisting of Quaternary and Tertiary strata generally have a lower geochemical background values than those of the outcrops areas (red) including intrusions and other formations, mainly due to the masking and decaying effects of these covers (Cheng, 2012b; Zuo et al., 2013; Cheng, 2014; Zuo et al., 2014). The weak or complicated geochemical anomalies in grassland area with low background or in granite area with high background bring the challenges for finding potential ore deposits. For instance, some ore deposits (e.g., Chaobuleng) located in the grassland area with low background value exhibit too weak anomalies to identify directly from geochemical pattern in Fig. 4. Similarly, those ore deposits occurring in granites area show insignificant geochemical anomaly patterns due to the interference of high background field (see in Fig. 4). Recent studies suggested that the effect of the covers on geochemical signals can be removed by nonlinear weak information extraction techniques such as the LSA and the S–A fractal filtering methods (Cheng, 2012a,b).

The LSA has a remarkable talent for delineating weak geochemical anomalies due to the fact that the realization of singularity index acts a high-pass filtering in processing geochemical data. To show this high-pass filtering talent, the spatial distribution of singularity indices is first obtained from the conventional LSA using moving average, where 3 square windows are defined with size of [3 km, 5 km, 7 km]. Note that the scale range of window size is determined by consideration of scale of local structure of interest (Cheng, 2007), and a small window size is chosen here since the resulting small-scale singularities may reflect the local anomalies associated with mineralization. From the singularity map in Fig. 6 it is observed that a number of weak anomaly patterns have been enhanced and identified from the complex background fields, particularly showing an intimately association with most of the ore deposits in the study area. These results demonstrated that LSA can identify weak geochemical anomalies and would assist in mapping mineral perspective. However, from signal filtering point of view, the result in Fig. 6 obtained from the conventional LSA still has somewhat imperfections. The area A and B for instance contain obvious residual interferences of high background field caused by granitic intrusions.

As discussed in Section 3, the proposed LSA calculates singularity index using a WMD scheme and theoretically possess a better ability for analyzing fractal/singular geochemical pattern compared with the conventional LSA algorithm. Singularity mapping result (Fig. 7) is then recalculated using the novel LSA based on WMD, where 3 scales (j=1, 2, 3) are used in order to make a comparison with the results of Fig. 6. Fig. 8 gives the log–log plots of approximation coefficients versus scales for testing points. The coefficient of determination (R^2) has been used to examine the goodness-of-fit of using regression analysis to fit the power–law function in log–log scale, and its mean value of all the sampled points has been recorded as 0.95, indicating reliable estimations of
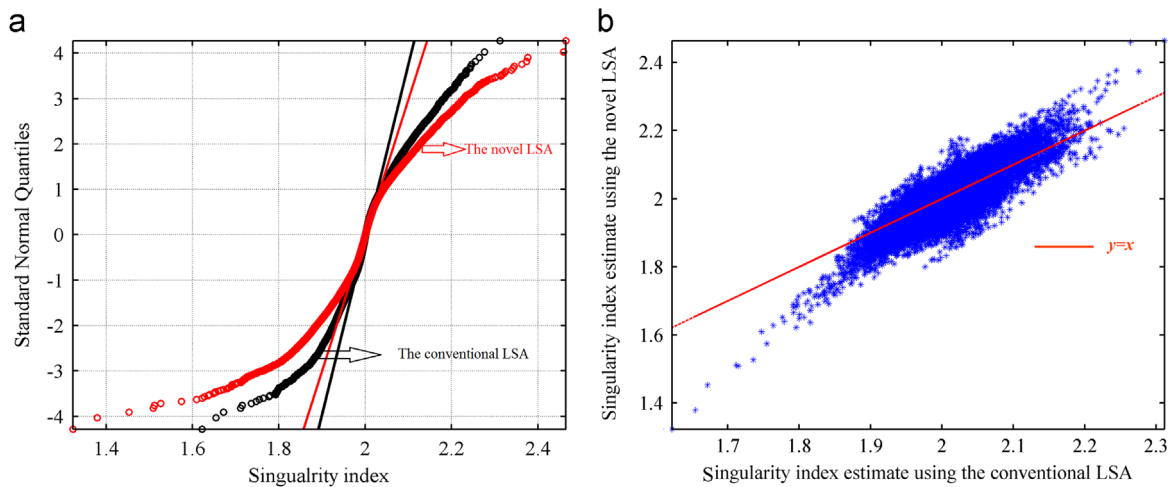
Fig. 10. (a) Q–Q plots of singularity estimates. (b) Plot of singularity estimates using the conventional LSA versus the novel LSA. (For interpretation of the references to color in this figure, the reader is referred to the web version of this article.)
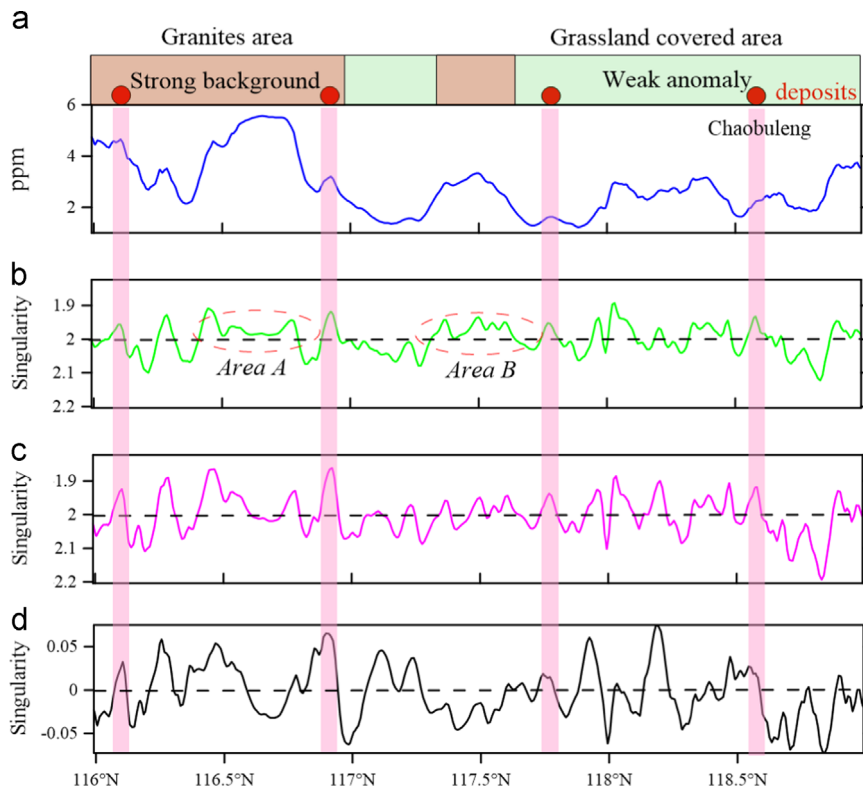

Fig. 11. Profiles showing the high-pass filtering performance of singularity index for identifying the weak anomalies. (a) Original profile anomaly of Fe$_2$O$_3$. (b) Singularity indices estimated by the conventional LSA. (c) Singularity indices estimated by the novel LSA. (d) The differences in the singularity estimates of the novel and conventional LSA.

singularity index. From the histogram statistic in Fig. 9, most of singularity indices are around $\alpha \approx 2$ indicating non-singular background field and approximately satisfy the normal distribution, while the (positive/negative) singular values seems to follow extreme-value distribution (e.g. Pareto and power–law) with long tails (see Q–Q plot in Fig. 10a).

In comparison with the conventional method (Fig. 6), on one hand, from the visual perspective the novel LSA obtains more distinct patterns indicating weak geochemical anomalies. The interferences of high background field caused by granites in such as area A and B have been removed more thoroughly in Fig. 7. On the other hand from the perspective of singularity estimates, the

histogram in Fig. 9 shows a bigger standard deviation of Fig. 7 than Fig. 6, and the novel LSA results in more points with $\alpha \approx 2$ (indicating background) as well as a longer and thicker tail of singularity distribution (indicating anomalies) (Fig. 10a). These facts suggest the novel LSA possesses a better ability of distinguishing the singular anomalies and background field. Moreover, from the plot of singularity estimates using the novel LSA versus conventional LSA, it can be appreciated that the novel LSA holds a better enhancing ability for estimating the singularity value of geochemical patterns. Note that when the two results are similar, a straight line ($y=x$) (red line in Fig. 10b) can be obtained. Such advantages of the novel LSA over the conventional method also

have been illustrated in profile plots in Fig. 11. Significantly, from the plot (Fig. 11d) of the difference in singularity estimates using the novel LSA (Fig. 11b) and the conventional LSA (Fig. 11c), it can be observed that the hidden geochemical anomalies caused by ore deposits show more distinct singularity signatures and higher singularity values. These results demonstrated that the novel LSA (using WMA) has an improved filtering ability than the conventional LSA for enhancing weak geochemical anomalies. In addition, Fig. 7 delineates more lineaments (linear anomaly patterns) in NWW or NE directions, since the wavelet analysis is more suitable for analyzing the non-isolated singularities compared with moving averaging method.

5. Conclusions

Wavelet-based multiscale decomposition (WMD) acts a powerful tool for analyzing the multiscale natures of geochemical pattern and provides a natural generalization of box-counting method for scaling analysis of fractal/singular geochemical measures. Based on the scaling property of wavelet approximation coefficients, a novel local singularity analysis (LSA) was presented in this contribution to detect the spatial distribution of singularities. It provides a nonlinear (weighted averaging) scheme for calculating the element density-value in density–area fractal modeling, in contrast with the conventional LSA using linear (averaging) scheme. The novel LSA using WMD can better model and quantify the (non-isolated) singularities in geochemical patterns resulted from mineralization, which was demonstrated in a case study dealing with geochemical data of Fe_2O_3. The singularity mapping result suggested that the novel LSA possesses a superior ability for enhancing and identifying weak geochemical anomalies associated with mineralization in covered area.

Acknowledgments

References

Afzal, P., Ahari, H.D., Omran, N.R., Aliyari, F., 2013a. Delineation of gold mineralized zones using concentration–volume fractal model in Qolqoleh gold deposit, NW Iran. Ore Geol. Rev. 55, 125–133.

Afzal, P., Alghalandis, Y.F., Khakzad, A., Moarefvand, P., Omran, N.R., 2011. Delineation of mineralization zones in porphyry Cu deposits by fractal concentration–volume modeling. J. Geochem. Explor. 108, 220–232.

Afzal, P., Harati, H., Alghalandis, Y.F., Yasrebi, A.B., 2013b. Application of spectrum–area fractal model to identify of geochemical anomalies based on soil data in Kahang porphyry-type Cu deposit, Iran. Chem. Erde Geochem. 73, 533–543.

Afzal, P., Khakzad, A., Moarefvand, P., Omran, N.R., Esfandiari, B., Alghalandis, Y.F., 2010. Geochemical anomaly separation by multifractal modeling in Kahang (Gor Gor) porphyry system, Central Iran. J. Geochem. Explor. 104, 34–46.

Agterberg, F., 1995. Multifractal modeling of the sizes and grades of giant and supergiant deposits. Int. Geol. Rev. 37, 1–8.

Agterberg, F., 2012. Multifractals and geostatistics. J. Geochem. Explor. 122, 113–122.

Agterberg, F., 2014. Geomathematics: Theoretical Foundations, Applications and Future Developments (Quantitative Geology and Geostatistics). vol. 18. Springer, Switzerland.

Agterberg, F.P., Cheng, Q., 1999. Introduction to special issue on "Fractals Multifractals". Comput. Geosci. 25, 947–948.

Ali, K., Cheng, Q., Chen, Z., 2007. Multifractal power spectrum and singularity analysis for modelling stream sediment geochemical distribution patterns to identify anomalies related to gold mineralization in Yunnan Province, South China. Geochem.: Explor. Environ. Anal. 7, 293–301.

Anand, R.R., Robertson, I.D., 2012. The role of mineralogy and geochemistry in forming anomalies on interfaces and in areas of deep basin cover: implications for exploration. Geochem.: Explor. Environ. Anal. 12, 45–66.

Arias, M., Gumiel, P., Martín-Izard, A., 2012. Multifractal analysis of geochemical anomalies: a tool for assessing prospectivity at the SE border of the Ossa Morena Zone, Variscan Massif (Spain). J. Geochem. Explor. 122, 101–112.

Arneodo, A., Bacry, E., Muzy, J., 1995. The thermodynamics of fractals revisited with wavelets. Phys. A: Stat. Mech. Appl. 213, 232–275.

Arneodo, A., Grasseau, G., Holschneider, M., 1988. Wavelet transform of multifractals. Phys. Rev. Lett. 61, 2281.

Bölviken, B., Stokke, P., Feder, J., Jössang, T., 1992. The fractal nature of geochemical landscapes. J. Geochem. Explor. 43, 91–109.

Basseville, M., Benveniste, A., Chou, K.C., Golden, S.A., Nikoukhah, R., Willsky, A.S., 1992. Modeling and estimation of multiresolution stochastic processes. IEEE Trans. Inf. Theory 38, 766–784.

Carranza, E.J.M., 2008. Geochemical Anomaly and Mineral Prospectivity Mapping in GIS (Handbook of Exploration and Environmental Geochemistry). vol. 11. Elsevier, Amsterdam.

Chamoli, A., Bansal, A.R., Dimri, V., 2007. Wavelet and rescaled range approach for the Hurst coefficient for short and long time series. Comput. Geosci. 33, 83–93.

Chen, G., Cheng, Q., Liu, T., Yang, Y., Mapping local singularities using magnetic data to investigate the volcanic rocks of the Qikou depression, Dagang oilfield, eastern China. Nonlinear Process. Geophys. 20, 2013, 501-511.

Chen, G., Cheng, Q., Zuo, R., Liu, T., Xi, Y., 2015. Identifying gravity anomalies caused by granitic intrusions in Nanling mineral district, China: a multifractal perspective. Geophys. Prospect. 63, 256–270.

Cheng, Q., 1995. Multifractal Modelling and Spatial Analysis with GIS: Gold Potential Estimation in the Mitchell-Sulphurets Area, Northwestern British Columbia. University of Ottawa, Canada.

Cheng, Q., 1999. Spatial and scaling modelling for geochemical anomaly separation. J. Geochem. Explor. 65, 175–194.

Cheng, Q., GIS-based multifractal anomaly analysis for prediction of mineralization and mineral deposits, In: (Ed.), J.R.H. (Ed.), GIS Applications in Earth Sciences, Geological Association of Canada, 2006, pp. 289-300.

Cheng, Q., 2007. Mapping singularities with stream sediment geochemical data for prediction of undiscovered mineral deposits in Gejiu, Yunnan Province, China. Ore Geol. Rev. 32, 314–324.

Cheng, Q., 2008. Non-linear theory and power–law models for information integration and mineral resources quantitative assessments. Math. Geosci. 40, 503–532.

Cheng, Q., 2012a. Ideas and methods for mineral resources integrated prediction in covered areas. Earth Sci. J. China Univ. Geosci. 6, 1109–1125.

Cheng, Q., 2012b. Singularity theory and methods for mapping geochemical anomalies caused by buried sources and for predicting undiscovered mineral deposits in covered areas. J. Geochem. Explor. 122, 55–70.

Cheng, Q., 2014. Vertical distribution of elements in regolith over mineral deposits and implications for mapping geochemical weak anomalies in covered areas. Geochem.: Explor. Environ. Anal. 14, 277–289.

Cheng, Q., 2015. Multifractal interpolation method for spatial data with singularities. J. South. Afr. Inst. Min. Metall. 115, 235–240.

Cheng, Q., Agterberg, F., Ballantyne, S., 1994. The separation of geochemical anomalies from background by fractal methods. J. Geochem. Explor. 51, 109–130.

Cheng, Q., Agterberg, F.P., 2009. Singularity analysis of ore-mineral and toxic trace elements in stream sediments. Comput. Geosci. 35, 234–244.

Cheng, Q., Xu, Y., Grunsky, E., 2000. Integrated spatial and spectrum method for geochemical anomaly separation. Nat. Resour. Res. 9, 43–52.

Cohen, D., Kelley, D., Anand, R., Coker, W., 2010. Major advances in exploration geochemistry, 1998–2007. Geochem. Explor. Environ. Anal. 10, 3–16.

Coker, W., 2010. Future research directions in exploration geochemistry. Geochem. Explor. Environ. Anal. 10, 75–80.

Daubechies, I., 1992. Ten lectures on wavelets. CBMS Lecture Notes Series. SIAM.

Davis, G.M., 1998. A wavelet-based analysis of fractal image compression. IEEE Trans. Image Process. 7, 141–154.

Evertszy, C.J., Mandelbrot, B.B., 1992. Multifractal measures. In: Peitgen, H.-O., Jurgens, H., Saupe, D. (Eds.), Chaos and Fractals. Springer-Verlag, New York.

Garrett, R., Reimann, C., Smith, D., Xie, X., 2008. From geochemical prospecting to international geochemical mapping: a historical overview. Geochem.: Explor. Environ. Anal. 8, 205–217.

Gonçalves, M.A., 2001. Characterization of geochemical distributions using multifractal models. Math. Geol. 33, 41–61.

Grossmann, A., Morlet, J., 1984. Decomposition of Hardy functions into square integrable wavelets of constant shape. SIAM J. Math. Anal. 15, 723–736.

Grunsky, E.C., 2010. The interpretation of geochemical survey data. Geochem.: Explor. Environ. Anal. 10, 27–74.

Kumar, P., Foufoula, E., 1997. Wavelet analysis for geophysical applications. Rev. Geophys. 35, 385–412.

Li, C., Ma, T., Shi, J., 2003. Application of a fractal method relating concentrations and distances for separation of geochemical anomalies from background. J. Geochem. Explor. 77, 167–175.

Mallat, S., 1989a. Multiresolution approximations and wavelet orthonormal bases of L^2(R). Trans. Am. Math. Soc. 315, 69–87.

Mallat, S., 1989b. A theory for multiresolution signal decomposition: the wavelet representation. IEEE Trans. Pattern Anal. Mach. Intell. 11, 674–693.

Mallat, S., 1999. A Wavelet Tour of Signal Processing. Academic Press, San Diego, CA.

Mallat, S., Hwang, W.L., 1992. Singularity detection and processing with wavelets. IEEE Trans. Inf. Theory 38, 617–643.

Mandelbrot, B., 1967. How long is the coast of Britain? Statistical self-similarity and fractional dimension. Science 156, 636–638.

Mandelbrot, B., 1983. The Fractal Geometry of Nature. W.H. Freeman and Company, New York.

Mandelbrot, B., 1989. Multifractal measures, especially for the geophysicist. Pure Appl. Geophys. 131, 5–42.

Morlet, J., Arens, G., Fourgeau, E., Glard, D., 1982. Wave propagation and sampling theory-Part I: complex signal and scattering in multilayered media. Geophysics 47, 203–221.

Muzy, J.-F., Bacry, E., Arneodo, A., 1994. The multifractal formalism revisited with wavelets. Int. J. Bifurc. Chaos 4, 245–302.

Singer, D.A., Kouda, R., 2001. Some simple guides to finding useful information in exploration geochemical data. Nat. Resour. Res. 10, 137–147.

Turcotte, D.L., 2002. Fractals in petrology. Lithos 65, 261–271.

Wang, W., Zhao, J., Cheng, Q., 2011. Analysis and integration of geo-information to identify granitic intrusions as exploration targets in southeastern Yunnan District, China. Comput. Geosci. 37, 1946–1957.

Wendt, H., Roux, S.G., Jaffard, S., Abry, P., 2009. Wavelet leaders and bootstrap for multifractal analysis of images. Signal Process. 89, 1100–1114.

Zuo, R., Cheng, Q., Agterberg, F., Xia, Q., 2009. Application of singularity mapping technique to identify local anomalies using stream sediment geochemical data, a case study from Gangdese, Tibet, western China. J. Geochem. Explor. 101, 225–235.

Zuo, R., Wang, J., Chen, G., Yang, M., 2014. Identification of weak anomalies: a multifractal perspective. J. Geochem. Explor. 154, 200–212.

Zuo, R., Xia, Q., Zhang, D., 2013. A comparison study of the C–A and S–A models with singularity analysis to identify geochemical anomalies in covered areas. Appl. Geochem. 33, 165–172.